Understanding Floquet Resonances in Ultracold Quantum Gas Scattering

Christoph Dauer, Axel Pelster, and Sebastian Eggert*
Physics Department and Research Center OPTIMAS, RPTU Kaiserslautern-Landau, 67663 Kaiserslautern, Germany

(Received 10 March 2025; accepted 1 July 2025; published 17 July 2025)

It is demonstrated that the effective scattering length can be highly manipulated via time-periodic driving of a short-range interparticle potential. By developing a Floquet-scattering theory we show that sharp Floquet resonances occur at which the effective interaction can be tuned to very large attractive or repulsive values. The resulting s-wave scattering length can be obtained in analytic form and the shape of these resonances is given by a simple formula describing how resonance position and width can be altered by the driving strength. Our approach allows the identification of the underlying physical mechanism of the scattering resonances as Floquet bound states with positive energies, which are dynamically created by the drive. This insight is valuable for a detailed analysis and uncovers a general resource for enhanced or reduced scattering in Floquet systems, as was recently confirmed experimentally.

DOI: 10.1103/47xs-223h

The physics of resonances is truly ubiquitous across different fields of science and in daily life, being crucial for the design of musical instruments, buildings, electrical circuits, and dance movements just to name a few. A resonance may be the most intimate physical phenomenon for humans since it can be directly experienced by sight, sound, or touch: a small amplitude of a time-periodic signal results in a huge effect when the frequency is just changed slightly to the "right" value. In modern physics the concept of resonances has broadened to also mean "energy matching." In fact, some very important discoveries in particle scattering, such as the Fano resonance [1,2] and the Feshbach resonance [3–8], do not involve any time periodicity at all. However, their effect is analogous: a slight change of incoming energy to the "right" value results in a huge increase of scattering. Not surprisingly, this property is indeed very useful in the context of tunable particle-particle interactions, which makes Feshbach-like interactions a valuable toolbox in studies of many-body quantum systems [3–22].

Although a Feshbach resonance does not require time-periodic fields, it is sometimes advantageous to dress the atomic states with light and/or microwave fields to access novel states at the right energies for added tunability [9–19]. However, in all those approaches an existing internal state or closed channel is required in the scattering process. This invites the question of whether it is possible to use only the time periodicity itself instead of an internal state, i.e., create a resonance in the classical sense by only matching the frequency of a time-periodic scattering length in a single channel. This is exactly the model described and analyzed below. Indeed, such a setup has been realized recently using ultracold ^{6}Li atoms [20], but to be fair an internal state was still involved for achieving a time-periodic interaction via an oscillating field [21]. Nonetheless, as we show here, this is just a technical detail and the origin of the observed resonances is purely dynamic. Hence, the Floquet-scattering approach [20] is a noteworthy extension in methodology. In this Letter, we uncover the underlying physical mechanism of such Floquet resonances from general time-periodic interactions and provide analytic formulas for the effective scattering, which are analyzed to give accurate predictions for location and width of the resonant behavior.

In our analysis we use Floquet theory [23–27], which is an interesting field in its own right for examining time-oscillating lattices and interactions in a variety of setups [28–62]. In the high frequency limit a steady state can often be realized, corresponding to Floquet engineering of an effective Hamiltonian. However, the understanding and utilization of resonances at lower frequencies still remain difficult because, generically, heating increases as more states are coupled. For the Floquet-scattering problem considered here, an incoming particle is subject to a local time-periodic potential, which is analogous to Floquet impurities in 1D [58–62]. In such cases, the incoming energy is not conserved, but there is no continuous "heating" from a single scattering process. Instead, the Floquet eigenstate can be explicitly calculated, which contains all information of the energy transfer into higher frequency modes in the steady state. Those losses correspond to a small imaginary part in the effective scattering length discussed below, so this is a special case where the

*Contact author: seggert@rptu.de

effective Floquet heating can be explicitly predicted and analyzed, paving the road to a systematic reduction.

The proposed setup can be modeled by a time-periodic s-wave scattering length,

$$a(t) = \bar{a} + a_1 \cos(\omega t), \tag{1}$$

where the amplitude is assumed to fulfill $|a_1| < |\bar{a}|$. In the center-of-mass frame of reference the s-wave collisions of ultracold atoms are described by the Hamiltonian

$$H(r,t) = \frac{\hbar^2}{2\mu}\left[-\Delta + 4\pi a(t)\delta^3(\mathbf{r})\frac{\partial}{\partial r}r\right] \tag{2}$$

in terms of the short-range pseudopotential formalism [63,64] along the radial coordinate r with reduced mass μ. There are no internal states and no assumptions are made about the underlying mechanism for the oscillating modulation $a(t)$, but it is instructive to consider prototypical values corresponding to ultracold ^{6}Li atoms in a magnetic field [20]: the collision energy at $T \sim 724$ nK is about a factor of 1000 smaller than the typical dimer energy $E_{\bar{a}} = \hbar^2/2\mu\bar{a}^2 \approx 2\pi\hbar \times 15$ MHz at $\bar{a} = 200a_0$ (Bohr radii). In the following we use units of $\hbar = \hbar^2/2\mu = 1$, which makes $E_{\bar{a}} = 1/\bar{a}^2$ the natural unit for frequencies and energies.

For a time-periodic Hamiltonian $H = H_0 + H_1 \cos \omega t$ the steady states $\psi(r,t) = e^{-i\epsilon t}\phi(r,t)$ can be found by Floquet theory [23–27], where ϵ is the Floquet eigenenergy. Using the Fourier transformation $H_n = \int_0^T dt e^{in\omega t} H(t)/T$ and the time-periodic Floquet mode $\phi(r,t) = \sum_n e^{-in\omega t}\phi_n(r)$, the time-dependent Schrödinger equation becomes an eigenvalue equation for the Floquet quasienergy ϵ,

$$H_0\phi_n(r) + H_1[\phi_{n-1}(r) + \phi_{n+1}(r)]/2 = (\epsilon + n\omega)\phi_n(r). \tag{3}$$

In terms of the pseudopotential from Eq. (2) this yields

$$(\Delta + \epsilon + n\omega)\phi_n = 4\pi\delta^3(\mathbf{r})\frac{\partial}{\partial r}r\left(\bar{a}\phi_n + a_1\frac{\phi_{n+1} + \phi_{n-1}}{2}\right). \tag{4}$$

We make the s-wave scattering ansatz [65]

$$\phi_n(r) = \delta_{n,0}\frac{\sin k_0 r}{k_0 r} + f_n\frac{e^{ik_n r}}{r} \tag{5}$$

with an incoming plane wave k_0 in the $n = 0$ channel. Note that for $r > 0$ the usual wave equation is fulfilled for each channel $H_0\phi_n = k_n^2\phi_n = (\epsilon + n\omega)\phi_n$, which fixes the Floquet energy $\epsilon = k_0^2$ and all scattered wave vectors $k_n = \sqrt{\epsilon + n\omega}$. For $n > 0$ the k_n are real, which correspond to open channels, where particles are lost, while $n < 0$ are bound states that lead to interesting resonances as we will see below. Using $\Delta(1/r) = -4\pi\delta^3(\mathbf{r})$ we arrive at the recursion relation

$$k_n f_n = L_n(k_{n+1}f_{n+1} + k_{n-1}f_{n-1}) + h_n, \tag{6}$$

$$\text{where } L_n = -\frac{ia_1 k_n}{2(1 + i\bar{a}k_n)}, \tag{7}$$

$$h_n = -iL_n(2\delta_{n,0}\bar{a}/a_1 + \delta_{|n|,1}). \tag{8}$$

For a numerical analysis we could stop at this point since the linear set of Eq. (6) can be efficiently solved with the convergence condition $f_{|n|\to\infty} \to 0$, as shown in Fig. 1. Interestingly, large resonances are observed for purely repulsive interactions $\bar{a} > 0$ and small amplitudes a_1, which we will analyze in the following.

First, we derive a continued fraction solution by dividing the recursion in Eq. (6) for $|n| > 1$ by the left-hand side, so it can be expressed in terms of fractions $g_n^\pm = k_n f_n/(L_n k_{n\mp1} f_{n\mp1})$ for positive $n > 1$ and negative $n < -1$, respectively,

$$g_n^\pm = \frac{1}{1 - L_n L_{n\pm1} g_{n\pm1}^\pm} = \frac{1}{1 - \frac{L_n L_{n\pm1}}{1 - \frac{L_{n\pm1}L_{n\pm2}}{1 - \frac{L_{n\pm2}L_{n\pm3}}{\ddots}}}}. \tag{9}$$

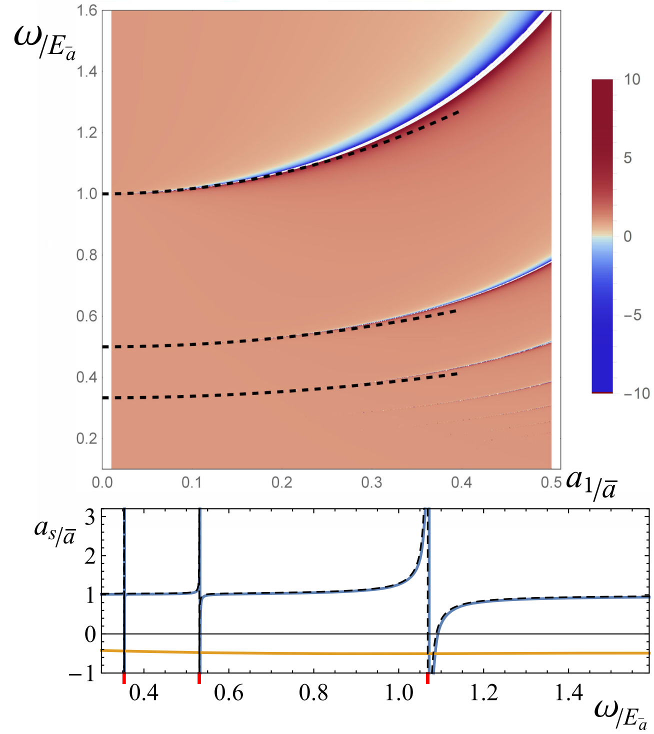

FIG. 1. Results for a_s from Eq. (11) for small driving amplitudes a_1 compared to the approximations in Eqs. (16)–(19) (dashed) for $\epsilon \to 0$. Top: real part as function of driving frequency ω and amplitude a_1. Bottom: imaginary part multiplied by 100 (orange) and real part (blue) for $a_1 = 0.2\bar{a}$. The positions of ω_m from Eq. (18) are marked red.

Here, we have inserted the definition of $g_n^{\pm}$ into Eq. (6) to obtain the relation in Eq. (9), which leads to the continued fraction solution [66–68] by straightforward iteration. Inserting $g_{\pm 2}^{\pm}$ from Eq. (9) into Eq. (6) for $n = 0, \pm 1$ the scattering amplitude is expressed in terms of an effective scattering length a_s (see Appendix A),

$$f_0 = -\frac{a_s}{1 + ik_0 a_s}, \tag{10}$$

$$\text{where } a_s = \bar{a} + a_1(L_1 g^+ + L_{-1} g^-)/2. \tag{11}$$

Here, $g^{\pm} = 1/(1 - L_{\pm 1} L_{\pm 2} g_{\pm 2}^{\pm})$ are given by the continued fractions for $n = \pm 1$ in Eq. (9). Hence, for the model in Eq. (2) an exact solution has been obtained, which can be evaluated to high order $n_{\max}$ in the continued fraction. In Figs. 1 and 2 $n_{\max} = 200$ was used. The effective scattering length a_s in Eq. (11) has two separate contributions from the periodic driving a_1. The term $a_1 L_1 g^+$ from the open channels $n > 0$ is of order a_1^2 and has both real and imaginary parts. This is due to the fact that particles are scattered into higher energy Fourier modes and are considered lost. The term $a_1 L_{-1} g^-$ from the closed channels $n < 0$ is purely real since $L_{n<0} \in \mathbb{R}$ and shows pronounced divergences if $\bar{a} > 0$. In fact, the form of the parameters L_n in Eq. (7) indicates singular points for $-i\bar{a}k_n = 1$. Using $k_n = \sqrt{n\omega + \epsilon}$, resonances will therefore occur for negative n close to $n\omega + \epsilon \sim -E_{\bar{a}}$ if $\bar{a} > 0$. Note that for $\bar{a} < 0$ no resonances are found, so we assume $\bar{a} > 0$ in the following.

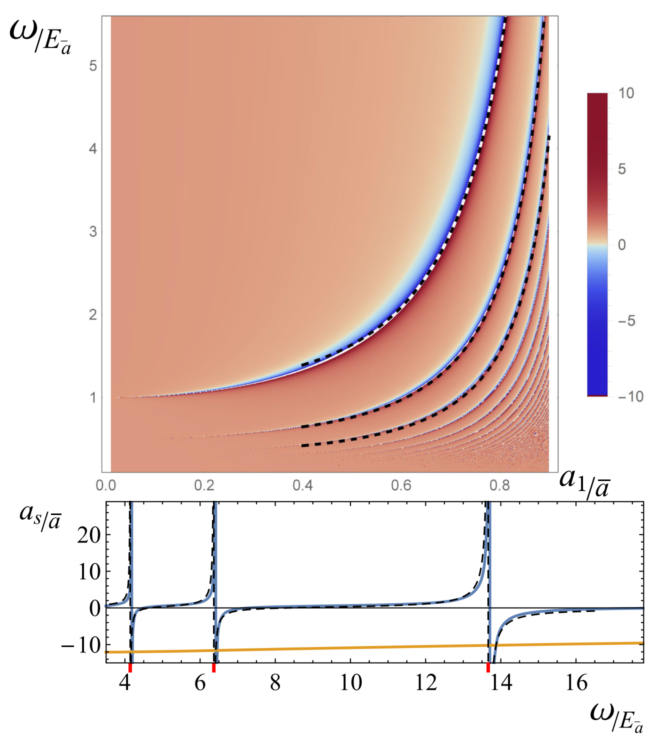

FIG. 2. Results for a_s from Eq. (11) for larger driving amplitudes a_1 compared to the approximations (black dashed) in Eqs. (16), (20), and (21) for $\epsilon \to 0$. Top: real part as function of frequency and amplitude. Bottom: imaginary part multiplied by 100 (orange) and real part (blue) for $a_1 = 0.9\bar{a}$. The positions of ω_m from Eq. (20) are marked red.

In order to unravel the physical origin of the resonances, we now propose an analysis in terms of Floquet bound states, which we define and predict below. It is well known that bound states are a valuable resource for strongly enhanced scattering resonances [65] in the context of Feshbach resonances [3–7], Fano resonances [1,2], or bound states in the continuum [69,70]. The mechanism for Floquet resonances is more involved, since in this case the bound state itself is generated dynamically, i.e., the periodic drive creates the bound state, tunes the resonance, and also provides the coupling, simultaneously.

Floquet bound states are defined as distinct solutions $|\phi^m\rangle$, labeled by the index $m = 1, 2, 3, \ldots$, to the Schrödinger equation, where only negative Fourier modes $n < 0$ are occupied. Using the ansatz

$$\phi_n^m(r) = D_n^m \frac{e^{-\kappa_n^m r}}{\kappa_n^m r} \tag{12}$$

with $\kappa_n^m = -ik_n^m = \sqrt{-\epsilon_m - n\omega}$ and the normalization condition $\sum_{n<0} |D_n^m|^2 (\kappa_n^m)^{-3} = 1/(2\pi) = \mathcal{N}^2$ [71], we obtain from Eq. (4)

$$(1 - \bar{a}\kappa_n^m) D_n^m = \frac{a_1}{2} \kappa_n^m (D_{n-1}^m + D_{n+1}^m), \quad \forall\ n < 0, \tag{13}$$

$$\text{where } \lim_{n \to -\infty} D_n^m = 0 \quad \text{and} \quad D_0^m = 0 \quad \forall\ m. \tag{14}$$

Note that Eq. (13) corresponds to Eq. (6) for $n < 0$ and $D_n^m = \kappa_n^m f_n$, but without any incoming or outgoing waves $D_0^m = f_0 = h_n = 0$. Analogous to a static Schrödinger equation, a set of localized solutions $|\phi^m\rangle$ can be found at discrete energies $\epsilon_m(\omega)$ with $m = 1, 2, 3, \ldots$, depending on frequency ω and amplitude a_1. Those Floquet bound states exist without any incoming wave $D_0^m = 0$ due to the periodic drive.

Before analyzing the corresponding eigenenergies ϵ_m in detail below, let us consider the implications. The effect of bound states in the continuum on scattering resonances was discussed in a number of different undriven systems [1–7,69,70]. In Appendix B we now present an explicit derivation of the effect of Floquet bound states, which follows a slightly different logic from the known static cases [1–7,69,70]. As a result, our theory accurately predicts all resonances in the effective scattering length in terms of the bound state energies $\epsilon_m(\omega)$ and the first components D_{-1}^m of the normalized bound states $|\phi^m\rangle$,

$$a_s = \bar{a} - \sum_m \frac{\pi a_1^2 |D_{-1}^m|^2}{\epsilon_m - \epsilon} + a_1 L_1 g^+/2. \tag{15}$$

This central result uncovers the physical origin of the observed resonances quantitatively in terms of individual bound state solutions. Note that the locations of the resonances are given by $\epsilon = \epsilon_m$, which are relevant if the bound state energies are positive, i.e., they represent bound states in the continuum [69,70]. Expanding the frequency dependence to linear order around the incoming energy $\epsilon_m \approx \epsilon + (\omega - \omega_m)\partial_\omega \epsilon_m$ for each m yields the standard form of the resonances [7],

$$a_s \approx \bar{a}\left(1 - \sum_m \frac{\Delta_m}{\omega - \omega_m}\right), \tag{16}$$

with identifying $\Delta_m = \pi a_1^2 |D_{-1}^m|^2 \bar{a}^{-1}/\partial_\omega \epsilon_m$, where the open-channel contribution $a_1 L_1 g^+/2$ has been omitted. The width Δ_m is defined [7] by the value $\omega = \omega_m + \Delta_m$, at which $a_s = 0$. We have tested and confirmed that the predicted positions of the resonances in Eqs. (15) and (16) from bound states agree with the continued fraction solution in Eq. (11). We now proceed to find analytic approximations for ω_m and Δ_m, which can be used for closed form quantitative predictions, that are plotted as dashed lines in Figs. 1 and 2.

For small a_1 a perturbative analysis of the bound-state solutions can be used for Eq. (13). To zeroth order in a_1 in Eq. (13) the energies are found by $\bar{a}\kappa_n^m = 1$, which is fulfilled for zeroth order energies $\epsilon_m = m\omega - E_{\bar{a}}$ and zeroth order eigenstates $D_n^m = \mathcal{N}\bar{a}^{-3/2}\delta_{m,-n}$. It may be surprising that bound states are predicted in zeroth order, i.e., for zero amplitude driving, but it is correct in the sense that resonances exist in the limit of infinitesimally small a_1 at frequencies $\omega_m = (E_{\bar{a}} + \epsilon)/m$. The zeroth order location of the resonances depends on the incoming energy ϵ and the order m, but remarkably the resonant bound wave function has the universal form $\mathcal{N}e^{-r\bar{a}}/r$ from Eq. (12) due to the underlying condition $\bar{a}\kappa_n^m = 1$, i.e., the size is always given by the average scattering length $\bar{a}$.

Next, the first-order correction in a_1 is obtained by inserting $D_{-m}^m = \mathcal{N}a^{-3/2}$ into Eq. (13), which yields the coefficients $D_{\pm 1-m}^m = \mathcal{N}\bar{a}^{-3/2}a_1/(2/\kappa_{\pm 1-m}^m - 2\bar{a})$ for $m = -n \pm 1$. Using $\kappa_{\pm 1-m}^m \approx \sqrt{E_{\bar{a}} \mp \omega}$, the second-order correction follows from Eq. (13) for $m = -n$,

$$\frac{1}{\bar{a}\sqrt{m\omega - \epsilon_m}} - 1 \approx \frac{a_1^2}{4}\left(\frac{\bar{a}\sqrt{E_{\bar{a}} + \omega}}{1 - \bar{a}\sqrt{E_{\bar{a}} + \omega}} + \frac{\bar{a}\sqrt{E_{\bar{a}} - \omega}}{1 - \bar{a}\sqrt{E_{\bar{a}} - \omega}}\right). \tag{17}$$

Solving this equation for ω_m for small scattering energies $\epsilon = \epsilon_m = 0$ gives all positions of the resonances up to order a_1^2,

$$\omega_m \approx \frac{E_{\bar{a}}}{m}\left(1 + \frac{a_1^2}{2\bar{a}^2}\left[2 + \sqrt{m(m+1)} - \sqrt{m(m-1)}\right]\right), \tag{18}$$

in the limit $k_0 \to 0$. The prediction of the resonance position can also be solved for the value of $\bar{a}$ as function of ω, which allows a direct comparison with the experimental analysis in Ref. [20] as discussed in Appendix D. The leading order of the respective width of the divergences as a function of a_1 results in [72]

$$\Delta_m = 2E_{\bar{a}}\left(\frac{a_1}{2\bar{a}}\right)^{2m} \prod_{j=1}^{m-1}\left(\frac{1}{\bar{a}\sqrt{E_{\bar{a}} - j\omega_m}} - 1\right)^{-2}, \tag{19}$$

in good agreement with the full solution in Fig. 1 even for relatively strong driving $a_1 = 0.2\bar{a}$. The small imaginary part from the unbound modes $a_1 L_1 g^+/2$ in Eq. (11) is also shown in Fig. 1, which can be well approximated by the expansion $\mathrm{Im}\, a_s \approx \mathrm{Im}\, a_1 L_1/2 = a_1^2\sqrt{\omega}/(4E_{\bar{a}} + 4\omega)$ to order a_1^2. For the leading resonance $\Delta_1 = (E_{\bar{a}}/2)(a_1/\bar{a})^2$ is the same order as the frequency shift, but for higher orders $m > 1$ the width $\Delta_m \propto a_1^{2m}$ becomes very small, so we need to consider stronger amplitudes beyond the perturbative approach.

Approaching larger $a_1 \to \bar{a}$ it turns out that the differences between neighboring coefficients in Eq. (13) rapidly become smaller, so that a continuous description in terms of differential equations can be used for the recursion relation. The details are presented in Appendix C with the outcome that the resonance positions and widths diverge with different power laws in the limit $a_1 \to \bar{a}$ according to

$$\omega_m = \frac{4}{a_1^2}\left(\frac{E_m}{2}\frac{a_1}{\bar{a} - a_1}\right)^{3/2}, \tag{20}$$

$$\Delta_m = \frac{F_m}{\bar{a}(\bar{a} - a_1)}, \tag{21}$$

where $E_m = 0.4380,\ 0.2632,\ 0.1976$ and $F_m = 0.212,\ 0.0628,\ 0.0313$ for the first three resonances. Note that in contrast to magnetic Feshbach resonances [7] the width and the position become independently tunable since there are now three adjustable parameters ω, $\bar{a}$, and a_1. The results of Eqs. (20) and (21) are plotted as dashed lines in Fig. 2 in good agreement with the exact solution from Eq. (11).

Analytical results are possible also in the limit of large frequencies $\omega \gg \omega_1 > E_{\bar{a}}$ in a regime that is beyond any resonance. In the recursion relation $|k_n| \to \infty$ for $n \neq 0$ in Eq. (7) leads to coefficients $L_n \to -a_1/(2\bar{a})$ independent of n. Therefore, also the continued fraction in Eq. (9) becomes independent of $n \neq 0$ and can be solved by a quadratic equation $g_n^{\pm} \to [(2\bar{a}^2)/a_1^2](1 - \sqrt{1 - a_1^2/\bar{a}^2})$. Inserting this into Eq. (11) we have

$$\lim_{\omega\to\infty} a_s = \bar{a}\sqrt{1 - \frac{a_1^2}{\bar{a}^2}}. \tag{22}$$

Hence, even for very large frequencies the driving does not average out, but reduces the magnitude of the effective scattering length. Note that the result in Eq. (22) is not limited to small a_1 or positive $\bar{a}$. It implies that the effective interaction can be reduced by high frequency driving, but never outside the range $\bar{a} \pm a_1$ of the time-dependent scattering in Eq. (1). In the high frequency limit, the behavior of experimental systems is typically stable over longer timescales, since there are no resonances and the losses become negligible. Hence, the result in Eq. (22) is suitable to be tested experimentally.

Last but not least, let us discuss the effects of higher harmonic terms in the time dependence of Eq. (1) with integer multiples of ω. This may be relevant in case the scattering length is modified using a field in Feshbach resonance $a(t)/a_{\rm bg} = 1 - \Delta/[B(t) - B_0]$ beyond a linear regime, but may also offer more tuning possibilities. The time dependence of the underlying field is normally under good control, so a perfect harmonic drive can be realized, as well as large higher harmonic contributions. Since the Hamiltonian is still time-periodic, the Floquet approach remains possible and the recursion relation can be modified in a straightforward way. Preliminary numerical results show that the principle structure of strong resonances is quite robust in the presence of higher harmonics, but changes quantitatively. This is also true for the imaginary part, which may be larger but may also be strongly suppressed. For a suppression, the phase and amplitude of the higher harmonics must be tuned so that the higher order amplitudes $f_{n>0}$ are very small, which is feasible in experiment [20]. We should mention at this point that an analysis of higher angular momentum Floquet scattering is also possible [72], in case larger energies become relevant.

In summary, we have analyzed the effect of a time-periodic scattering length [20] in quantum many-body systems. The resulting interactions are highly tunable by the frequency and the amplitude of the drive. In particular, we predict very large effective scattering amplitudes, which can be positive or negative as a result of a small oscillating repulsive potential. This paves the way for future applications of switching many-body interactions using only slight changes in frequency and small amplitudes. The added tuning capabilities of three independent parameters in the Floquet resonance and the possibility to quickly and accurately adjust the driving frequency facilitates an extended toolbox for time-dependent protocols and multiple particle species. A analytic form of the scattering amplitude was derived and analyzed. Both for small and large driving amplitudes a_1 we obtain approximations for the location and width of resonances, which fit well with the exact results. Equally important, we uncovered the underlying mechanism of the strong resonance behavior, namely bound Floquet states with positive energies, which are created dynamically by the drive. This insight has proven to be valuable for obtaining analytic predictions, but also opens the door for a systematic search, analysis, and creation of such bound Floquet states in related systems for enhanced tuning possibilities, changing interactions from small to large values with slight parameter changes.

Acknowledgments—We thank A. Guthmann and A. Widera for inspiring discussions. Furthermore, we acknowledge financial support by the Deutsche Forschungsgemeinschaft (DFG, German Research Foundation) via the Collaborative Research Center SFB/TR185 (Project No. 277625399).

Data availability—The data that support the findings of this Letter are not publicly available upon publication because it is not technically feasible and/or the cost of preparing, depositing, and hosting the data would be prohibitive within the terms of this research project. The data are available from the authors upon reasonable request.

[1] U. Fano, Effects of configuration interaction on intensities and phase shifts, Phys. Rev. **124**, 1866 (1961).
[2] A. E. Miroshnichenko, S. Flach, and Y. S. Kivshar, Fano resonances in nanoscale structures, Rev. Mod. Phys. **82**, 2257 (2010).
[3] S. Inouye, M. R. Andrews, J. Stenger, H.-J. Miesner, D. M. Stamper-Kurn, and W. Ketterle, Observation of Feshbach resonances in a Bose-Einstein condensate, Nature (London) **392**, 151 (1998).
[4] E. Timmermans, P. Tommasini, M. Hussein, and A. Kerman, Feshbach resonances in atomic Bose-Einstein condensates, Phys. Rep. **315**, 199 (1999).
[5] V. Vuletić, A. J. Kerman, C. Chin, and S. Chu, Observation of low-field Feshbach resonances in collisions of Cesium atoms, Phys. Rev. Lett. **82**, 1406 (1999).
[6] C. Chin, V. Vuletić, A. J. Kerman, and S. Chu, High resolution Feshbach spectroscopy of Cesium, Phys. Rev. Lett. **85**, 2717 (2000).
[7] C. Chin, R. Grimm, P. Julienne, and E. Tiesinga, Feshbach resonances in ultracold gases, Rev. Mod. Phys. **82**, 1225 (2010).
[8] R. A. Duine and H. T. C. Stoof, Atom–molecule coherence in Bose gases, Phys. Rep. **396**, 115 (2004).
[9] P. O. Fedichev, Y. Kagan, G. V. Shlyapnikov, and J. T. M. Walraven, Influence of nearly resonant light on the scattering length in low-temperature atomic gases, Phys. Rev. Lett. **77**, 2913 (1996).
[10] M. Theis, G. Thalhammer, K. Winkler, M. Hellwig, G. Ruff, R. Grimm, and J. Hecker Denschlag, Tuning the scattering length with an optically induced Feshbach resonance, Phys. Rev. Lett. **93**, 123001 (2004).
[11] G. Thalhammer, M. Theis, K. Winkler, R. Grimm, and J. Hecker Denschlag, Inducing an optical Feshbach resonance via stimulated Raman coupling, Phys. Rev. A **71**, 033403 (2005).
[12] T. L. Nicholson, S. Blatt, B. J. Bloom, J. R. Williams, J. W. Thomsen, J. Ye, and P. S. Julienne, Optical Feshbach resonances: Field-dressed theory and comparison with experiments, Phys. Rev. A **92**, 022709 (2015).
[13] O. Thomas, C. Lippe, T. Eichert, and H. Ott, Experimental realization of a Rydberg optical Feshbach resonance in a quantum many-body system, Nat. Commun. **9**, 2238 (2018).
[14] A. M. Kaufman, R. P. Anderson, T. M. Hanna, E. Tiesinga, P. S. Julienne, and D. S. Hall, Radio-frequency dressing of

multiple Feshbach resonances, Phys. Rev. A **80**, 050701(R) (2009).

[15] P. Zhang, P. Naidon, and M. Ueda, Independent control of scattering lengths in multicomponent quantum gases, Phys. Rev. Lett. **103**, 133202 (2009).

[16] T. V. Tscherbul, T. Calarco, I. Lesanovsky, R. V. Krems, A. Dalgarno, and J. Schmiedmayer, Rf-field-induced Feshbach resonances, Phys. Rev. A **81**, 050701(R) (2010).

[17] T. M. Hanna, E. Tiesinga, and P. S. Julienne, Creation and manipulation of Feshbach resonances with radiofrequency radiation, New J. Phys. **12**, 083031 (2010).

[18] D. J. Papoular, G. V. Shlyapnikov, and J. Dalibard, Microwave-induced Fano-Feshbach resonances, Phys. Rev. A **81**, 041603(R) (2010).

[19] D. J. Owens, T. Xie, and J. M. Hutson, Creating Feshbach resonances for ultracold molecule formation with radiofrequency fields, Phys. Rev. A **94**, 023619 (2016).

[20] A. Guthmann, F. Lang, L. M. Kienesberger, S. Barbosa, and A. Widera, Floquet-engineering of Feshbach resonances in ultracold gases, arXiv:2503.05454.

[21] D. H. Smith, Inducing resonant interactions in ultracold atoms with a modulated magnetic field, Phys. Rev. Lett. **115**, 193002 (2015).

[22] A. G. Sykes, H. Landa, and D. S. Petrov, Two- and three-body problem with Floquet-driven zero-range interactions, Phys. Rev. A **95**, 062705 (2017).

[23] J. H. Shirley, Solution of the Schrödinger equation with a Hamiltonian periodic in time, Phys. Rev. **138**, B979 (1965).

[24] H. Sambe, Steady states and quasienergies of a quantum-mechanical system in an oscillating field, Phys. Rev. A **7**, 2203 (1973).

[25] M. Grifoni and P. Hänggi, Driven quantum tunneling, Phys. Rep. **304**, 229 (1998).

[26] M. Holthaus, Floquet engineering with quasienergy bands of periodically driven optical lattices, J. Phys. B **49**, 013001 (2016).

[27] A. Eckardt, Colloquium: Atomic quantum gases in periodically driven optical lattices, Rev. Mod. Phys. **89**, 1 (2017).

[28] D. H. Dunlap and V. M. Kenkre, Dynamic localization of a charged particle moving under the influence of an electric field, Phys. Rev. B **34**, 3625 (1986).

[29] A. Eckardt, C. Weiss, and M. Holthaus, Superfluid-insulator transition in a periodically driven optical lattice, Phys. Rev. Lett. **95**, 260404 (2005).

[30] H. Lignier, C. Sias, D. Ciampini, Y. Singh, A. Zenesini, O. Morsch, and E. Arimondo, Dynamical control of matter-wave tunneling in periodic potentials, Phys. Rev. Lett. **99**, 220403 (2007).

[31] C. Sias, H. Lignier, Y. P. Singh, A. Zenesini, D. Ciampini, O. Morsch, and E. Arimondo, Observation of photon-assisted tunneling in optical lattices, Phys. Rev. Lett. **100**, 040404 (2008).

[32] A. Zenesini, H. Lignier, D. Ciampini, O. Morsch, and E. Arimondo, Coherent control of dressed matter waves, Phys. Rev. Lett. **102**, 100403 (2009).

[33] T. Salger, S. Kling, T. Hecking, C. Geckeler, L. Morales-Molina, and M. Weitz, Directed transport of atoms in a Hamiltonian quantum ratchet, Science **326**, 1241 (2009).

[34] T. Kitagawa, E. Berg, M. Rudner, and E. Demler, Topological characterization of periodically driven quantum systems, Phys. Rev. B **82**, 235114 (2010).

[35] S. E. Pollack, D. Dries, R. G. Hulet, K. M. F. Magalhães, E. A. L. Henn, E. R. F. Ramos, M. A. Caracanhas, and V. S. Bagnato, Collective excitation of a Bose-Einstein condensate by modulation of the atomic scattering length, Phys. Rev. A **81**, 053627 (2010).

[36] J. Dalibard, F. Gerbier, G. Juzeliūnas, and P. Öhberg, Colloquium: Artificial gauge potentials for neutral atoms, Rev. Mod. Phys. **83**, 1523 (2011).

[37] I. Vidanović, A. Balaž, H. Al-Jibbouri, and A. Pelster, Nonlinear Bose-Einstein-condensate dynamics induced by a harmonic modulation of the s-wave scattering length, Phys. Rev. A **84**, 013618 (2011).

[38] J. Struck, C. Ölschläger, M. Weinberg, P. Hauke, J. Simonet, A. Eckardt, M. Lewenstein, K. Sengstock, and P. Windpassinger, Tunable gauge potential for neutral and spinless particles in driven optical lattices, Phys. Rev. Lett. **108**, 225304 (2012).

[39] P. Hauke, O. Tieleman, A. Celi, C. Ölschläger, J. Simonet, J. Struck, M. Weinberg, P. Windpassinger, K. Sengstock, M. Lewenstein, and A. Eckardt, Non-Abelian gauge fields and topological insulators in shaken optical lattices, Phys. Rev. Lett. **109**, 145301 (2012).

[40] M. Aidelsburger, M. Atala, M. Lohse, J. T. Barreiro, B. Paredes, and I. Bloch, Realization of the Hofstadter Hamiltonian with ultracold atoms in optical lattices, Phys. Rev. Lett. **111**, 185301 (2013).

[41] M. S. Rudner, N. H. Lindner, E. Berg, and M. Levin, Anomalous edge states and the bulk-edge correspondence for periodically driven two-dimensional systems, Phys. Rev. X **3**, 031005 (2013).

[42] T. Wang, X.-F. Zhang, F. E. A. dos Santos, S. Eggert, and A. Pelster, Tuning the quantum phase transition of bosons in optical lattices via periodic modulation of the s-wave scattering length, Phys. Rev. A **90**, 013633 (2014).

[43] N. Goldman and J. Dalibard, Periodically driven quantum systems: Effective Hamiltonians and engineered gauge fields, Phys. Rev. X **4**, 1 (2014).

[44] G. Jotzu, M. Messer, R. Desbuquois, M. Lebrat, T. Uehlinger, D. Greif, and T. Esslinger, Experimental realization of the topological Haldane model with ultracold fermions, Nature (London) **515**, 237 (2014).

[45] W. Cairncross and A. Pelster, Parametric resonance in Bose-Einstein condensates with periodic modulation of attractive interaction, Europhys. J. D **68**, 106 (2014).

[46] N. Fläschner, D. Vogel, M. Tarnowski, B. S. Rem, D. S. Lühmann, M. Heyl, J. C. Budich, L. Mathey, K. Sengstock, and C. Weitenberg, Observation of dynamical vortices after quenches in a system with topology, Nat. Phys. **14**, 1 (2017).

[47] L. W. Clark, A. Gaj, L. Feng, and C. Chin, Collective emission of matter-wave jets from driven Bose–Einstein condensates, Nature (London) **551**, 356 (2017).

[48] N. Mann, M. Reza Bakhtiari, F. Massel, A. Pelster, and M. Thorwart, Driven Bose-Hubbard model with a parametrically modulated harmonic trap, Phys. Rev. A **95**, 043604 (2017).

[49] B. Wang, F. N. Ünal, and A. Eckardt, Floquet engineering of optical solenoids and quantized charge pumping along tailored paths in two-dimensional Chern insulators, Phys. Rev. Lett. **120**, 243602 (2018).
[50] A. J. E. Kreil, H. Y. Musiienko-Shmarova, S. Eggert, A. A. Serga, B. Hillebrands, D. A. Bozhko, A. Pomyalov, and V. S. L'vov, Tunable space-time crystal in room-temperature magnetodielectrics, Phys. Rev. B **100**, 020406(R) (2019).
[51] J. H. V. Nguyen, M. C. Tsatsos, D. Luo, A. U. J. Lode, G. D. Telles, V. S. Bagnato, and R. G. Hulet, Parametric excitation of a Bose-Einstein condensate: From Faraday waves to granulation, Phys. Rev. X **9**, 011052 (2019).
[52] Z. Fedorova (Cherpakova), C. Jörg, C. Dauer, F. Letscher, M. Fleischhauer, S. Eggert, S. Linden, and G. von Freymann, Limits of topological protection under local periodic driving, Light Sci. Appl. **8**, 63 (2019).
[53] T. Wang, S. Hu, S. Eggert, M. Fleischhauer, A. Pelster, and X.-F. Zhang, Floquet-induced superfluidity with periodically modulated interactions of two-species hardcore bosons in a one-dimensional optical lattice, Phys. Rev. Res. **2**, 013275 (2020).
[54] S. Fazzini, P. Chudzinski, C. Dauer, I. Schneider, and S. Eggert, Nonequilibrium Floquet steady states of time-periodic driven Luttinger liquids, Phys. Rev. Lett. **126**, 243401 (2021).
[55] Simon B. Jäger, Jan Mathis Giesen, Imke Schneider, and Sebastian Eggert, Dissipative dicke time crystals: An atom's point of view, Phys. Rev. A **110**, L010202 (2024).
[56] Z. Fedorova, C. Dauer, A. Sidorenko, S. Eggert, J. Kroha, and S. Linden, Dissipation engineered directional filter for quantum ratchets, Phys. Rev. Res. **3**, 013260 (2021).
[57] E. Wamba, A. Pelster, and J. R. Anglin, Mapping as a probe for heating suppression in periodically driven quantum many-body systems, arXiv:2108.07171.
[58] D. Thuberg, S. A. Reyes, and S. Eggert, Quantum resonance catastrophe for conductance through a periodically driven barrier, Phys. Rev. B **93**, 180301(R) (2016).
[59] S. A. Reyes, D. Thuberg, D. Pérez, C. Dauer, and S. Eggert, Transport through an AC-driven impurity: Fano interference and bound states in the continuum, New J. Phys. **19**, 043029 (2017).
[60] D. Thuberg, E. Muñoz, S. Eggert, and S. A. Reyes, Perfect spin filter by periodic drive of a ferromagnetic quantum barrier, Phys. Rev. Lett. **119**, 267701 (2017).
[61] F. Hübner, C. Dauer, S. Eggert, C. Kollath, and A. Sheikhan, Floquet-engineered pair and single particle filter in the Fermi Hubbard model, Phys. Rev. A **106**, 043303 (2022).
[62] F. Hübner, C. Dauer, S. Eggert, C. Kollath, and A. Sheikhan, Momentum-resolved Floquet-engineered pair and single-particle filter in the Fermi-Hubbard model, Phys. Rev. A **108**, 023307 (2023).
[63] K. Huang and C. N. Yang, Quantum-mechanical many-body problem with hard-sphere interaction, Phys. Rev. **105**, 767 (1957).
[64] R. Stock, A. Silberfarb, E. L. Bolda, and I. H. Deutsch, Generalized pseudopotentials for higher partial wave scattering, Phys. Rev. Lett. **94**, 023202 (2005).
[65] H. Friedrich, *Scattering Theory* (Springer, Berlin, 2015).
[66] C. Brezinski, *History of Continnued Fractions and Padé Approximations* (Springer, Berlin, 1991).
[67] C. Simmendinger, A. Wunderlin, and A. Pelster, Analytical approach for the Floquet theory of delay differential equations, Phys. Rev. E **59**, 5344 (1999).
[68] D. Martinez, Floquet theory and continued fractions for harmonically driven systems, Ph.D. thesis, The University of Texas, Austin, 2003, http://hdl.handle.net/2152/756.
[69] H. Friedrich and D. Wintgen, Physical realization of bound states in the continuum, Phys. Rev. A **31**, 3964 (1985).
[70] H. Friedrich and D. Wintgen, Interfering resonances and bound states in the continuum, Phys. Rev. A **32**, 3231 (1985).
[71] For the scalar product time averaging and space integration are used, so different Fourier components $n \neq n'$ are orthogonal.
[72] Christoph Dauer, Resonances in interacting Floquet systems and dynamic transport phenomena, Doctoral thesis, University of Kaiserslautern, 2022, 10.26204/KLUEDO/8782.
[73] A. M. Ishkhanyan, Exact solution of the Schrödinger equation for the inverse square root potential $v_0/\sqrt{x}$, Europhys. Lett. **112**, 10006 (2015).
[74] G. Zürn, T. Lompe, A. N. Wenz, S. Jochim, P. S. Julienne, and J. M. Hutson, Precise characterization of ^{6}Li Feshbach resonances using trap-sideband-resolved rf spectroscopy of weakly bound molecules, Phys. Rev. Lett. **110**, 135301 (2013).

End Matter

Appendix A: Effective scattering amplitude—In order to derive Eq. (10) we apply Eq. (6) for $n = \pm 1$,

$$\begin{aligned} k_{\pm1} f_{\pm1} &= L_{\pm1}(k_0 f_0 + k_{\pm2} f_{\pm2} - i) \\ &= L_{\pm1}(k_0 f_0 + k_{\pm1} f_{\pm1} L_{\pm2} g^{\pm}_{\pm2} - i), \end{aligned} \tag{A1}$$

where we have used $g^{\pm}_{\pm2} = k_{\pm2} f_{\pm2}/(L_{\pm2} k_{\pm1} f_{\pm1})$. Solving this for $k_{\pm1} f_{\pm1}$ gives

$$\begin{aligned} k_{\pm1} f_{\pm1} &= L_{\pm1}(k_0 f_0 - i)/(1 - L_{\pm1} L_{\pm2} g^{\pm}_{\pm2}) \\ &= L_{\pm1}(k_0 f_0 - i) g^{\pm}, \end{aligned} \tag{A2}$$

where $g^{\pm} = 1/(1 - L_{\pm1} L_{\pm2} g^{\pm}_{\pm2})$ are given by the continued fraction in Eq. (9) for $n = \pm 1$. For $n = 0$ it follows from Eqs. (6) and (A2) that

$$\begin{aligned} k_0 f_0 &= L_0(k_1 f_1 + k_{-1} f_{-1} - 2i\bar{a}/a_1) \\ &= L_0[(k_0 f_0 - i)(L_1 g^+ + L_{-1} g^-) - 2i\bar{a}/a_1] \\ &= 2L_0((k_0 f_0 - i)(a_s - \bar{a}) - i\bar{a})/a_1 \\ &= \frac{-k_0}{1 + ik_0\bar{a}}[ik_0 f_0(a_s - \bar{a}) + a_s], \end{aligned} \tag{A3}$$

where we have used Eq. (7) and defined

$$a_s - \bar{a} = a_1(L_1 g^+ + L_{-1} g^-)/2 \quad \text{(A4)}$$

as in Eq. (11). Finally, solving Eq. (A3) for f_0 gives Eq. (10).

Appendix B: Floquet Feshbach resonance—The goal of this section is to evaluate the scattering contribution $a_1 L_{-1} g^-$ from the closed channels in terms of the bound-state solutions $|\phi^m\rangle$ and ϵ_m as defined in Eqs. (12)–(14). The calculation leading to Eq. (11) defines the effective scattering length a_s, but we now use the ansatz that the bound Fourier modes $\phi_{n<0}$ in Eq. (5) may be written as a superposition of orthonormal bound-state solutions $|\phi^m\rangle$ in Eq. (12),

$$f_n \frac{e^{ik_n r}}{r} = \sum_m A_m \phi_n^m(r) \quad \text{for } n < 0. \quad \text{(B1)}$$

In order to determine the expansion coefficients A_m we insert this ansatz into Eq. (4) and use the recursion relation in Eq. (13) to obtain

$$\sum_m (\epsilon - \epsilon_m) A_m \phi_n^m = \left[\frac{\overleftrightarrow{\partial}}{\partial r} r\phi_0\right] 2\pi a_1 \delta^3(\mathbf{r}) \delta_{n,-1}. \quad \text{(B2)}$$

Here, the double arrow indicates a Hermitian operator acting both to the right and to the left [72], which becomes important when taking scalar products after multiplying both sides with $\phi_n^{m'*}(r)$. After integrating both sides [71], the orthonormality of solutions $\sum_{n<0} \int d^3\mathbf{r} \phi_n^{m'*}(r) \phi_n^m(r) = \delta_{m',m}$ gives

$$A_{m'} = \frac{2\pi a_1 D_{-1}^{m'*}}{\epsilon_{m'} - \epsilon}(1 + ik_0 f_0). \quad \text{(B3)}$$

Finally, the relation $k_{-1} f_{-1} = i \sum_m A_m D_{-1}^m$ from taking $r \to 0$ in Eq. (B1) can be inserted into Eq. (A2), so that

$$L_{-1} g^- = -\sum_m \frac{2\pi a_1 |D_{-1}^m|^2}{\epsilon_m - \epsilon}. \quad \text{(B4)}$$

Inserting this into Eq. (11) yields the important result Eq. (15) of the main text. Note that each Floquet bound state gives rise to exactly one resonance independent from all others. The expansion in Eq. (B1) in terms of orthogonal eigenstates works so well because they are defined in the presence of the drive, i.e., there cannot be any additional coupling via exchange of photons between them. Hence, each of them couples separately to the incoming and scattered waves and contributes one resonance.

Appendix C: Continuum limit—A continuum theory [22] can be defined in terms of a variable $x = -n/A \geq 0$, where we have rescaled the index according to

$$A = \left(\frac{a_1^2 \omega}{4}\right)^{1/3}, \qquad \mathcal{D}\left(x = -\frac{n}{A}\right) = (-1)^n D_n. \quad \text{(C1)}$$

Using $D_{n+1} - 2D_n + D_{n-1} \approx \partial_x^2 \mathcal{D}(x)/A^2$ the bound-state recursion relation in Eq. (13) becomes a differential equation,

$$\left(-\frac{1}{\sqrt{x - \tilde{\epsilon}_m}} - \frac{\partial^2}{\partial^2 x}\right)\mathcal{D}(x) = -E\mathcal{D}(x), \quad \text{(C2)}$$

$$\text{where } E = 2A^2 \frac{\bar{a} - a_1}{a_1}. \quad \text{(C3)}$$

Here, we have used $a_1 \kappa_n^m/(2A^2) = \sqrt{x - \tilde{\epsilon}_m}$ and defined $\tilde{\epsilon}_m = \epsilon_m/(\omega A)$. The rescaled Eq. (C2) has only solutions for discrete dimensionless eigenvalues [73], which are given by $E_m = 0.4380$, 0.2632, 0.1976, 0.1617, 0.1386 for the first five numerical solutions of $\epsilon_m = 0$. Inserting those values into Eq. (C3) and solving for ω we obtain the corresponding conditions for the resonant frequency for each solution,

$$\omega_m = \frac{4}{a_1^2}\left(\frac{E_m}{2}\frac{a_1}{\bar{a} - a_1}\right)^{3/2}, \quad \text{(C4)}$$

which shows a divergence as $a_1 \to \bar{a}$. Hence, the rescaling A also becomes quite large in that limit, which in turn justifies the continuous ansatz. The corresponding width the continuum limit yields [72]

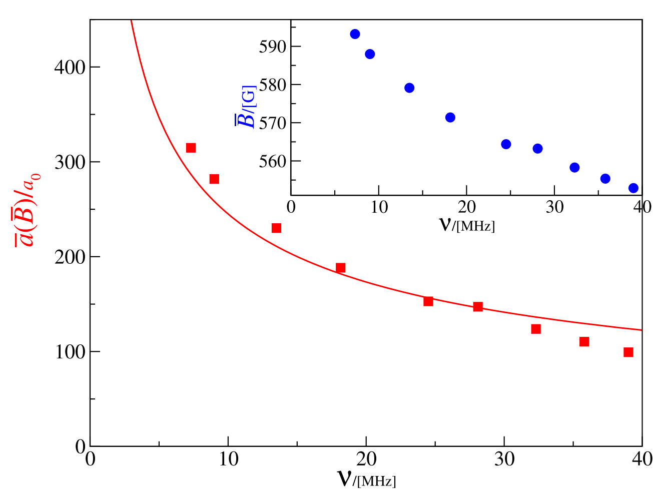

FIG. 3. The resonance positions of $\bar{a}$ (red squares) corresponding to the measured fields $\bar{B}$ (inset) from Ref. [20] compared to Eq. (D1) (solid line) as a function of frequency.

$$\Delta_m = \frac{F_m}{\bar{a}(\bar{a} - a_1)}, \tag{C5}$$

where the first three coefficients are given by $F_m = 0.212, 0.0628, 0.0313$.

Appendix D: Comparison with experiment—In Ref. [20] the leading ($m = 1$) resonance positions were studied experimentally using the broad ^{6}Li Feshbach resonance [74] in a time-periodic field $B(t) = \bar{B} + B_1 \cos \omega t$ with $B_1 \ll \bar{B}$. The values of the field $\bar{B}$ for Floquet resonance positions at different frequencies $2\pi\nu = \omega_1$ are shown in the inset of Fig. 3 from the original data in Ref. [20]. These fields can be converted to average scattering lengths $\bar{a}$ using the experimental data in Supplemental Material of Ref. [74], which are shown as red squares in Fig. 3. To compare to our theoretical calculations we use Eq. (18) for $m = 1$ to leading order and solve for the resonance values of $\bar{a}$ as a function of $\nu = \omega_1/(2\pi)$, which gives

$$\bar{a} = \sqrt{\frac{\hbar}{2\mu} \frac{1}{2\pi\nu}}, \tag{D1}$$

where we have reinstated all units and used the effective mass $2\mu = m_{^6\mathrm{Li}}$ for the red curve in Fig. 3, which agrees without any adjustable parameters. Some discrepancies are to be expected since all internal states were neglected in our model.